Experimental observations of mechanical dilation at the onset of gas flow in Callovo-Oxfordian claystone

ROBERT CUSS[1]*, JON HARRINGTON[1], RICHARD GIOT[2] & CHRISTOPHE AUVRAY[2]

[1]*Transport Properties Research Laboratory, British Geological Survey, Keyworth, Nottingham, NG12 5GG, UK*

[2]*LAEGO-ENSG-Université de Lorraine, Rue du Doyen Marcel Roubault, B.P. 40, F-54501 Vandœuvre-Lès-Nancy, France*

**Corresponding author (e-mail: rjcu@bgs.ac.uk)*

Abstract: Understanding the mechanisms controlling the advective movement of gas and its potential impact on a geological disposal facility (GDF) for radioactive waste is important to performance assessment. In a clay-based GDF, four primary phenomenological models can be defined to describe gas flow: (i) diffusion and/or solution within interstitial water; (ii) visco-capillary (or two-phase) flow in the original porosity of the fabric; (iii) flow along localized dilatant pathways (micro-fissuring); and (iv) gas fracturing of the rock. To investigate which mechanism(s) control the movement of gas, two independent experimental studies on Callovo-Oxfordian claystone (COx) have been undertaken at the British Geological Survey (BGS) and LAEGO–ENSG Nancy (LAEGO).

The study conducted at BGS used a triaxial apparatus specifically designed to resolve very small volumetric (axial and radial) strains potentially associated with the onset of gas flow. The LAEGO study utilized a triaxial setup with axial and radial strains measured by strain gauges glued to the sample. Both studies were conducted on COx at *in situ* stresses representative of the Bure Underground Research Laboratory (URL), with flux and pressure of gas and water carefully monitored throughout long-duration experiments.

A four-stage model has been postulated to explain the experimental results. Stage 1: gas enters at the gas entry pressure. Gas propagation is along dilatant pathways that exploit the pore network of the material. Around each pathway the fabric compresses, which may lead to localized movement of water away from the pathways. Stage 2: the dendritic flow path network has reached the mid-plane of the sample, resulting in acceleration of the observed radial strain. During this stage, outflow from the sample also develops. Stage 3: gas has reached the backpressure end of the sample with end-to-end movement of gas. Dilation continues, indicating that gas pathway numbers have increased. Stage 4: gas-fracturing occurs with a significant tensile fracture forming, resulting in failure of the sample.

Both studies clearly showed that as gas started to move through the COx, the sample underwent mechanical dilation (i.e. an increase in sample volume). Under *in situ* conditions, the onset of dilation (micro-fissuring) is a necessary precursor for the advective movement of gas.

In a geological disposal facility (GDF) for radioactive waste, corrosion of ferrous materials under anoxic conditions, combined with the radioactive decay of the waste and the radiolysis of water, will lead to the formation of hydrogen. A full understanding of the migration behaviour of this gas is of fundamental importance to the development of a GDF. If the rate of gas production exceeds the rate of gas diffusion within the pores of the barrier or host rock, a discrete gas phase will form (Wikramaratna *et al.* 1993; Ortiz *et al.* 2002; Weetjens & Sillen 2006). If this occurs, capillary restrictions (Aziz & Settari 1979) on the movement of gas will result in the build-up of pressure to a critical value when pressure becomes sufficiently large for it to enter the surrounding material and move through advective processes.

To accurately predict the movement of gas through argillaceous materials (Neretnieks 1984; Kreis 1991; Askarieh *et al.* 2000; Ekeroth *et al.* 2006; Smart *et al.* 2006) , it is first necessary to define the correct conceptual model that best represents the empirical data. In a clay-based GDF, four primary phenomenological models can be defined to describe gas flow, as proposed by Marschall *et al.* (2005; Fig. 1): (i) gas movement by solution and/or diffusion, governed by Henry's and Fick's laws respectively, within interstitial fluids along prevailing hydraulic gradients; (ii) gas flow in the original porosity of the fabric, governed by a generalized form of Darcy's Law, commonly referred to as visco-capillary (or two-phase) flow; (iii) gas flow along localized dilatant pathways (micro-fissuring),

From: NORRIS, S., BRUNO, J., CATHELINEAU, M., DELAGE, P., FAIRHURST, C., GAUCHER, E. C., HÖHN, E. H., KALINICHEV, A., LALIEUX, P. & SELLIN, P. (eds) 2014. *Clays in Natural and Engineered Barriers for Radioactive Waste Confinement*. Geological Society, London, Special Publications, **400**, 507–519.
First published online May 8, 2014, http://dx.doi.org/10.1144/SP400.26

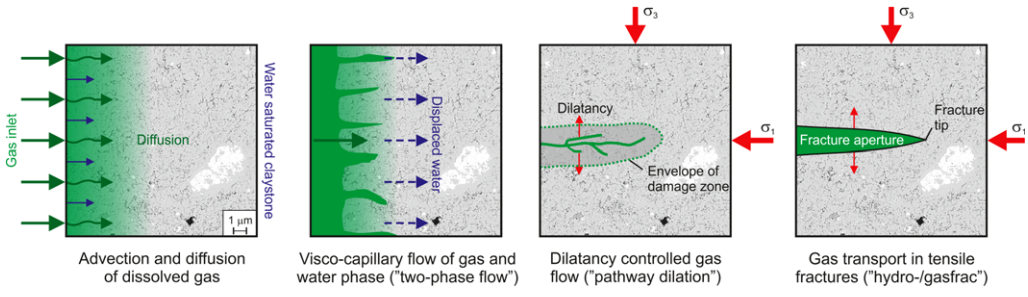

Fig. 1. Description of the four main processes of gas movement in clays (after Marschall *et al.* 2005).

which may or may not interact with the continuum stress field, the permeability of which is dependent on an interplay between local gas pressure and the effective stress state; and (iv) gas flow along macro fractures similar in form to those observed in hydrofracture activities during reservoir stimulation, where fracture initiation occurs when the gas pressure exceeds the sum of the minor principle stress and tensile strength. For engineering problems such as radioactive waste disposal, underground gas storage and carbon dioxide sequestration, most interest is focused on understanding the processes and mechanisms governing the advective transport of gas (mechanisms ii–iv).

There is now a growing body of evidence (Horseman *et al.* 1996, 2004; Harrington & Horseman 1999; Angeli *et al.* 2009; Harrington *et al.* 2009, 2012) that in the case of plastic clays and in particular bentonite, classic concepts of porous-medium two-phase flow are inappropriate. Flow through dilatant pathways has been shown in a number of argillaceous materials (Horseman & Harrington 1994; Harrington & Horseman 1997, 1999; Ortiz *et al.* 1996, 2002; Gallé & Tanai 1998; Horseman *et al.* 1999; Autio *et al.* 2006; Angeli *et al.* 2009). The pathways are pressure-induced and their aperture is a function of their internal gas pressure and structural constraints within the clay. However, the exact mechanisms controlling gas entry, flow and pathway sealing in clay-rich media are not fully understood and the 'memory' of such pathways could impair barrier performance.

To investigate which mechanism(s) control the advective movement of gas, two independent experimental studies on Callovo-Oxfordian claystone (COx) have been undertaken at the British Geological Survey (BGS, UK) and LAEGO–ENSG–Université de Lorraine (Nancy, France).

Experimental apparatus at BGS

The bespoke stress-path permeameter (SPP, Fig. 2) was used to investigate water and gas (helium) flow in COx from the Bure Underground Research Laboratory (URL) in the eastern part of the Paris Basin under *in situ* conditions (see Table 1 for test material parameters and experimental boundary conditions). See Cuss & Harrington (2010, 2011); Cuss *et al.* (2012) for a full description of the test apparatus and experimental history.

The triaxial SPP testing rig (Fig. 2) was designed to observe sample volume changes during flow experiments conducted along an evolving stress path; please note that the results presented here were for a static triaxial boundary condition. The apparatus had a thick-walled pressure vessel that imposed a confining pressure (12.5 MPa) through the compression of glycerol by an ISCO syringe pump. The test sample (Fig. 2c) was cylindrical and of 56 mm diameter and 82 mm length. The sample was jacketed in a Hoek sleeve, which had been thinned to reduce compressibility and had three brass plates cemented to the outside of the jacket. Three pressure-balanced devices (dash-pots) allowed direct measurement of the displacement of these plates to give radial displacement. The sample was axially loaded by an Enerpac hydraulic ram driven by an ISCO syringe pump, giving a stress of 13 MPa in the axial direction. Axial displacement was directly recorded by a Mitutoyo digital micrometer. The pore-pressure system had two ISCO syringe pumps; one acted as an injection pump and the other maintained constant back-pressure (4.5 MPa). A test was conducted using stages of constant pressure or constant-flow pressure ramps in the injection system in order to initiate gas or water flow. The experimental rig was completed by a number of pressure sensors, thermocouples and a digital acquisition system, which logged data every 2 min.

One experimental uncertainty in transport testing is the short-circuiting of the flow system along the jacket of the test sample. The addition of a 6-mm-wide, 2-mm-deep, porous stainless-steel annular filter along the outer edge of each platen (Fig. 2b) allowed porewater pressure to be monitored and discounted unwanted sidewall flow. These two

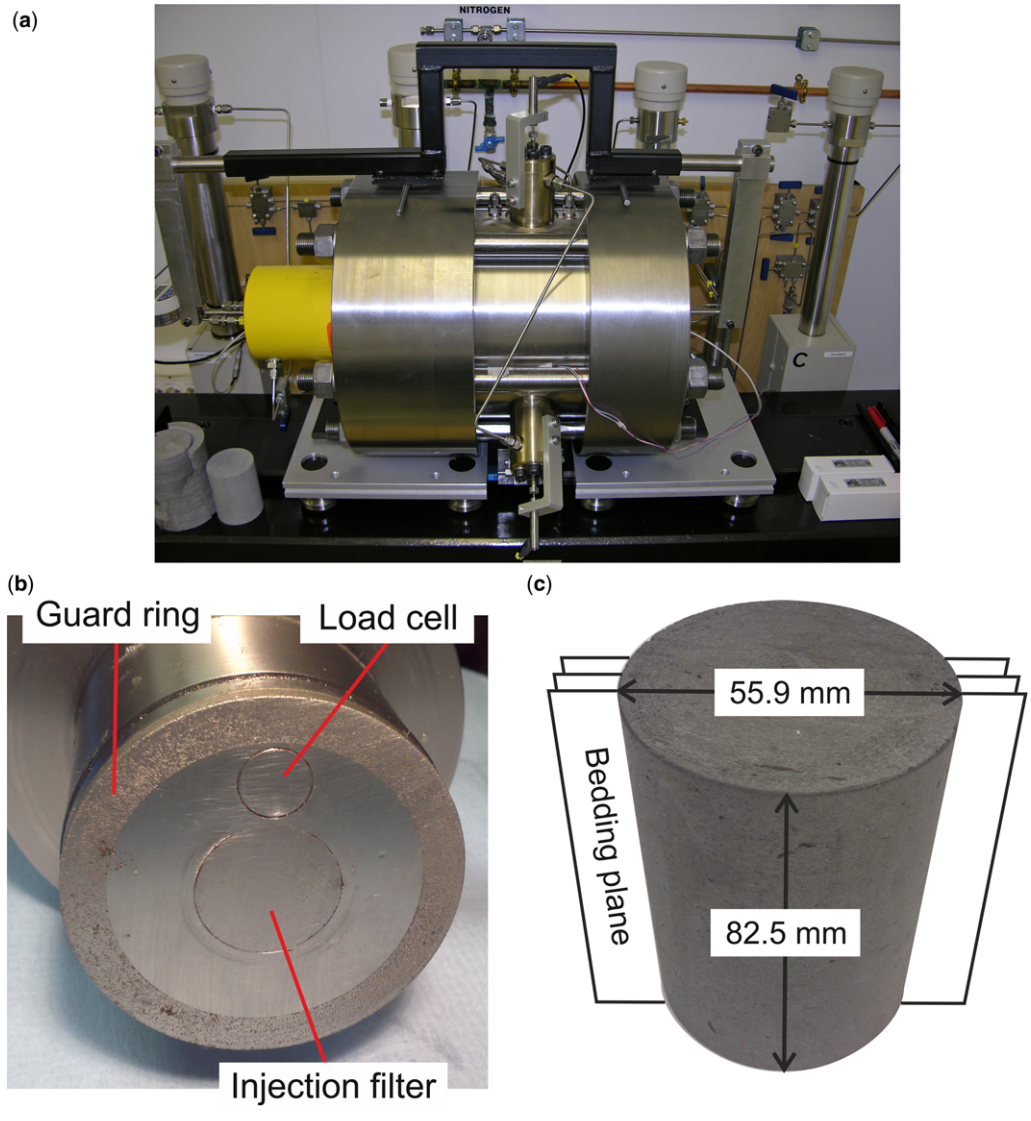

Fig. 2. Triaxial test setup: (**a**) triaxial SPP apparatus; (**b**) end platen showing the injection filter and guard ring arrangement; (**c**) sample of COx prior to testing.

guard rings (Harrington *et al.* 2003) were each connected to a pressure transducer and the complete guard-ring system (filter, pipework and pressure sensor) was saturated with water and flushed in order to eliminate gas from the system. The inlet/outlet filter was comprised of a porous disc 20 mm in diameter and 2 mm depth. The control board of the apparatus allowed the guard rings to be either connected to the injection system to assist in hydration, or isolated to give an independent measure of pore pressure. As well as being able to eliminate sidewall flow as a possible transport mechanism, the guard rings meant pore pressure was measured at four different points on the test sample (injection pressure, injection guard-ring pressure, backpressure, back guard-ring pressure), therefore providing data on hydraulic anisotropy within the sample.

The SPP was used to conduct experiments on COx under *in situ* stress conditions. Wenk *et al.* (2008) reports clay (25–55 wt%), 23–44% carbonates and 20–31% silt (essentially quartz + feldspar). Clay minerals are reported to include illite and illite-smectite with subordinate kaolinite

Table 1. *Description of pre-test COx material properties and experimental boundary conditions*

		Triaxial geometry BGS	Triaxial geometry LAEGO	Units
Sample properties	Sample reference	SPP_COx-2	EST28906-6	
	Location	Bure URL, France	Bure URL, France	
	Borehole/drill core	OHZ1201/EST30341	EST28906	
	Core direction	Parallel to bedding	Normal to bedding	
	Average length	82.45 ± 0.03	76.69	mm
	Average diameter/width	55.85 ± 0.04	37.89	mm
	Volume	2.020×10^{-4}	8.647×10^{-5}	m^3
	Average weight	495.02	203.22	g
	Density	2.451	2.35	g cc^{-1}
	Grain density	2.7	2.71	g cc^{-1}
	Moisture weight	28.7	11.95	g
	Moisture content	6.2	6.3	%
	Dry weight	466	191.27	g
	Dry density	2.31	2.21	g cc^{-1}
	Void ratio	0.174		
	Porosity	14.8	18.5	%
	Degree of saturation	96	85	%
Experimental boundary conditions	Confining pressure	12.5	12	MPa
	Axial load	13	12	MPa
	Pore pressure	4.5–10.5	4/6	MPa
	Back pressure	4.5	3.5	MPa
	Pore fluid chemistry	Chemically balanced pore fluid†		

*An assumed specific gravity for the mineral phases of 2.70 Mg m^{-3} (Zhang *et al.* 2007) was used in these calculations.
†227 mg l^{-1} Ca^{2+}, 125 mg l^{-1} Mg^{2+}, 1012 mg l^{-1} Na^{+}, 35.7 mg l^{-1} K^{+}, 1266 mg l^{-1} SO_4^{2-}, 4.59 mg l^{-1} Si, 9.83 mg l^{-1} SiO_2, 13.5 mg l^{-1} Sr, 423 mg l^{-1} total S, 0.941 mg l^{-1} total Fe.

and chlorite. Upon receipt of the preserved T1-cell core barrels at BGS, the material was catalogued and stored under refrigerated conditions of 4 °C to minimize biological and chemical degradation. The test sample was prepared by dry machine-lathing parallel to bedding, and the ends were ground flat and parallel giving an 82.45 mm length sample. The starting water saturation was 96%, with the early stages of testing designed to raise this to full saturation. Table 1 summarizes the geotechnical properties of the starting material; on completion of the full test programme the sample was seen to have saturation close to 100%.

Test SPP_COx-2 lasted a total of 566 days, with the results from the first 320 days up to the point of attainment of near-steady-state gas flow presented in this paper (see Table 2 for a summary of test boundary conditions). At the start of testing the sample was loaded to the *in situ* conditions at Bure with a confining pressure of 12.5 MPa, axial stress of 13 MPa and a pore pressure of 4.5 MPa. The initial stage of testing was designed to resaturate the sample fully and lasted 47 days. The sample exhibited a negative volumetric strain (i.e. volume increase) due to swelling. A constant head hydraulic test was subsequently performed in order to both remove any residual gas from the sample and to define the baseline hydraulic properties (permeability and specific storage) of the sample; this stage of testing lasted 79 days. This was followed by a gas injection experiment.

Experimental apparatus at LAEGO–ENSG–Université de Lorraine (Nancy)

A laboratory test was developed at LAEGO–ENSG–Université de Lorraine (Nancy) in order to give rise to dilatancy-controlled gas flow (Fig. 1, mode iii) and to gas transport in tensile fractures (Fig. 1, mode iv). The apparatus (Fig. 3) allowed gas flow to be monitored in samples submitted to a stress state close to the natural stress state under different gas pressures. The occurrence of either/both transport modes (iii, iv) induces an increase of gas and water flow as well as dilatant sample strain. The measurement of flow and strain should make it possible to distinguish between either transport mode.

The experimental apparatus consisted of a triaxial load cell, equipped with two fluid circuits, one for water and one for gas. Pressure sensors were installed on both circuits to measure the evolution of gas and water pressures at different places throughout the entire test history.

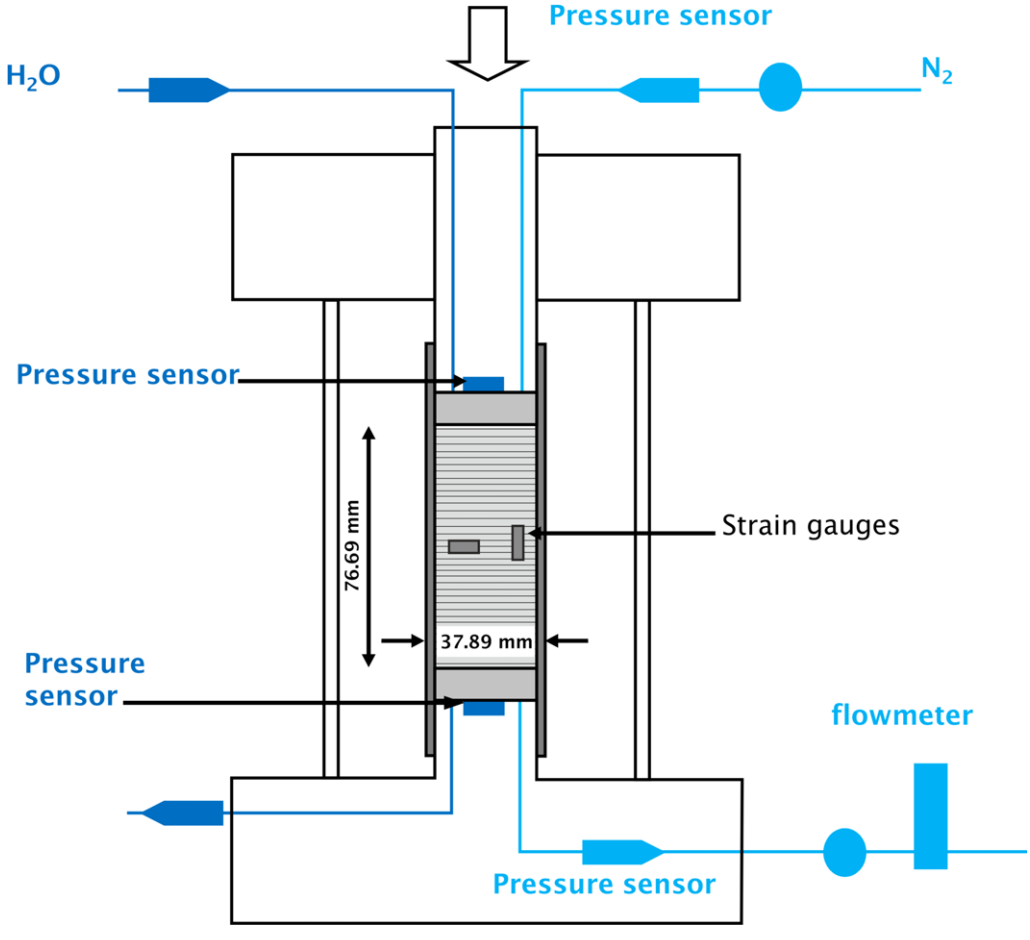

Fig. 3. Schematic of the experimental setup at LAEGO.

The presence of both gas and water required specific flow meters, with respective precisions of 10^{-3} g h^{-1} and 10^{-4} l min^{-1}. Strain gauges were glued directly on the sample to continuously measure axial and lateral deformations of the sample. Hydrostatic (for confining pressure) and pore (during saturation phase) pressures were produced through ISCO syringe pumps. Gas pressure was produced by a third ISCO syringe pump coupled with an oil-to-gas exchanger located between the pump and the cell. The oil-to-gas exchanger comprised a reservoir consisting of two compartments separated by a hermetic membrane; pressure was generated in the compartment containing oil and transmitted, through the membrane, to the compartment containing the gas.

The test consisted of three steps:

(1) Saturation of the sample. A sample was saturated under a hydrostatic stress state of 12 MPa with a difference between injected upstream and downstream pressures of 0.5 MPa. This step could typically last two to three months, depending on the sample. Axial and transversal strains were measured with strains gauges.

(2) Increase of gas pressure. An initial gas pressure of 4 MPa was applied upstream to the sample. Strains and outflowing gas and water flux were measured; pressure sensors were located along the system to check for constant gas pressure. After stabilization of strain and flux, a second gas pressure of 6 MPa was applied, followed by a third gas pressure level of 8 MPa.

(3) A third step can be considered if both the metrology and the sample allow it: a deviatoric stress can be applied to induce rupture (or the maximal stress of 20 MPa of the experimental apparatus).

Table 2. *Summary of experimental history conducted at BGS showing stage number, description of stage, axial stress and confining stress*

Stage number	Description	Axial stress (MPa)	Confining stress (MPa)	Injection pore pressure (MPa)	Test time at start (days)	Length of stage (days)
1	Saturation and swelling	12.5	11.5	4.5	0.1	21.7
2	Equilibration	13.0	12.5	4.5	21.8	26.1
3a	Hydraulic testing	13.0	12.5	8.5	47.9	50.1
3b	Hydraulic testing	13.0	12.5	4.5	98.0	29
4a	Gas injection ramp (constant flow)	13.0	12.5	4.5–9.5	127.0	35.3
4b	Gas injection at constant pressure	13.0	12.5	9.5	162.3	25.5
4c	Gas injection ramp (constant flow)	13.0	12.5	9.5–10	187.8	22.2
4d	Gas injection at constant pressure	13.0	12.5	10	210.0	26.1
4e	Gas injection ramp (constant flow)	13.0	12.5	10–10.5	236.1	18.9
4f	Gas injection at constant pressure	13.0	12.5	10.5	255.0	320.0

The axis of the sample was oriented normal to the bedding plane, with a diameter of 37.89 mm and a height of 76.69 mm. The carbonate content was measured as 18%, initial saturation was 85%, with the first stage of the test designed to achieve full saturation. The saturation at the end of the test could not be determined as the sample was contaminated with confining fluid while the test was decommissioned. Table 1 summarizes the geotechnical properties of the starting material.

Test results at BGS

Gas testing began on day 131, with a constant-flow pressure ramp that raised the injection gas pressure from 4.5 to 9.5 MPa over a 35-day period (see Fig. 4a). Gas pressure was held constant for 25 days and no indication of flow was seen. A second pressure ramp with a duration of 22 days was initiated on day 187, raising the gas injection pressure to 10 MPa. The pressure was held constant for 26 days and again no evidence of gas flow was seen. A final pressure ramp was initiated on day 236, raising the gas injection pressure to 10.5 MPa over a 19-day period.

Gas entry was subsequently identified as first occurring on day 220, with an anomalous reading in the load cell at day 221.875 signifying that gas had propagated to this sink. No further gas propagation seems to have occurred during this constant-pressure stage.

By day 241 it was apparent that gas had started flowing, so it took a total of 119 days to carefully raise the injection pressure from *in situ* levels to that necessary to initiate gas flow.

A second response was seen in the load cell reading at day 237.32. This suggests that the first gas propogation event pathway(s) closed. A day after the load cell reading response the water pressure in the guard ring started to increase (see Fig. 5a); a day after this, the first indication of deformation at the mid-plane was seen (Fig. 5b). The following day, the water pressure in the backpressure guard ring started to increase. These changes are interpreted as being a hydromechanical response to the onset of gas migration and the displacement of water from the injection guard ring due to the geometry of the test apparatus.

Gas migration was seen to result in an accelerated dilation at the mid-plane at around day 255 (see Figs 4b & 5b) that cannot be described by the mechanical response of a change in effective stress alone. The sample behaviour suggests that gas had migrated along dilational pathways. Gas reached the backpressure guard ring by around day 273. Marked deformation occurred following the onset of gas flow with a total of 48 μm of length dilation occurring and an average radial dilation of *c.* 16 μm. This represents a total volumetric strain of 0.18%, or a 360 μl change in sample volume. During the remainder of the gas tests, the radial strain trace exhibited the same functional form as that for the outflow of gas from the sample, providing conclusive proof that gas flow was accompanied by dilation of the COx.

Dilatancy observed at LAEGO–ENSG–Université de Lorraine (Nancy)

The sample of COx was fully saturated under an isotropic stress of 12 MPa, close to the *in situ* state of stress for Bure, for four months. Axial and radial strains were measured using strain gauges glued to the sample, and gas and water flux and pressure were monitored. An initial gas pressure of 4 MPa was applied to the sample for 24 days (Fig. 6a). The pressure downstream of the sample initially decreased and then stabilized after ten days, with

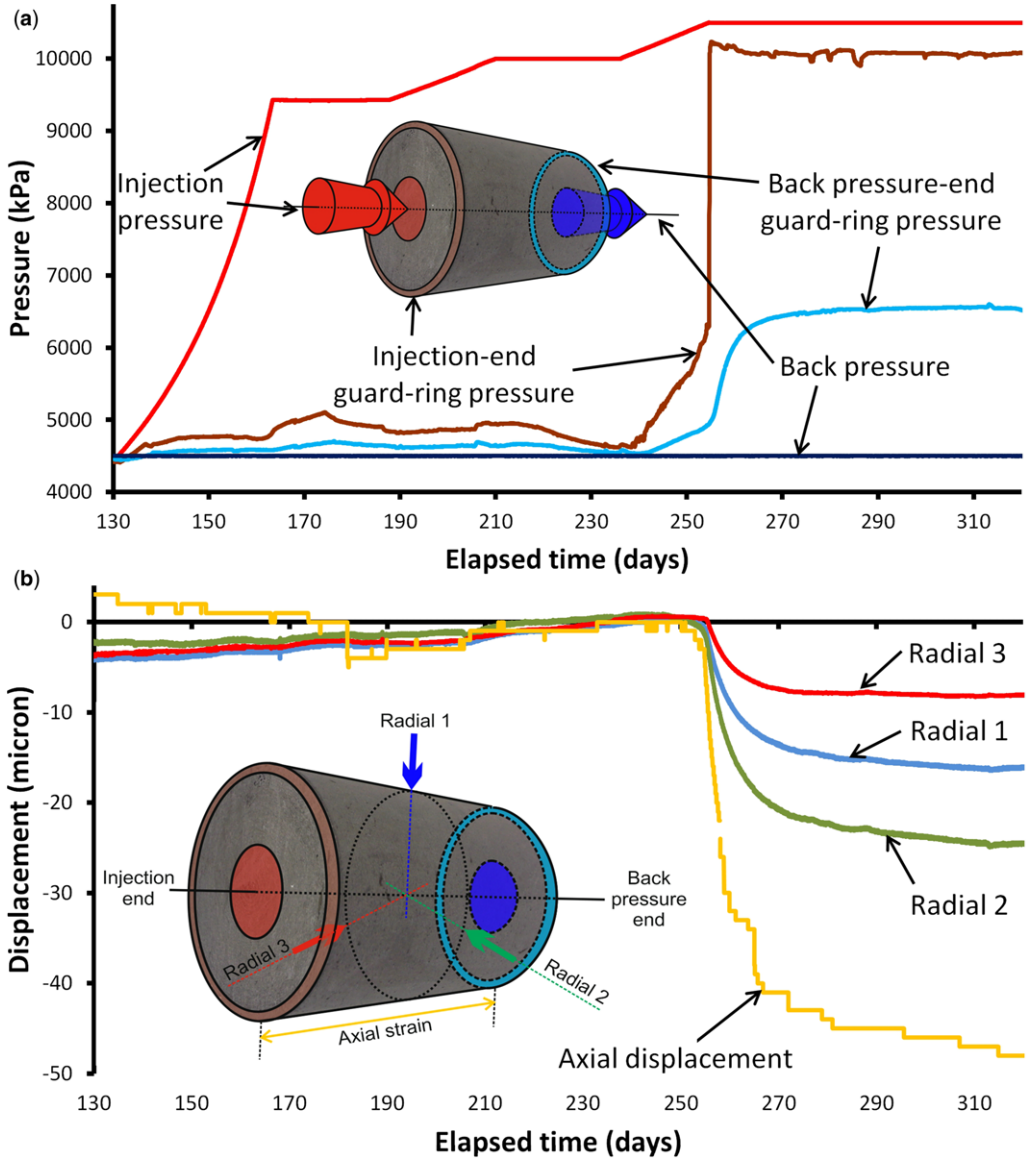

Fig. 4. Experimental results from the BGS test: (**a**) pressure recorded at four points within the experimental setup; (**b**) deformation recorded at four locations on the sample, clearly showing dilation.

the axial strain (Fig. 6b) stabilizing four days later. On day 25, the gas pressure was increased to 6 MPa, at which point the downstream pressure suddenly increased to 4.2 MPa. Thereafter, back-pressure decreased steadily without showing any conspicuous sign of stabilizing. In parallel, the axial and lateral strains increased rapidly and appeared to stabilize by day 38. This was followed by an acceleration of axial strain up to day 42. Alongside these accelerating strains, upstream and downstream gas pressures dropped suddenly, which seems to indicate that the sample underwent micro-cracking. These observations show that the onset of gas migration is described by model (iii), corresponding to gas micro-fissuring of the saturated sample. The maximum pressure that was reached seems lower than that conventionally measured, and the micro-fissuring phase corresponds to an

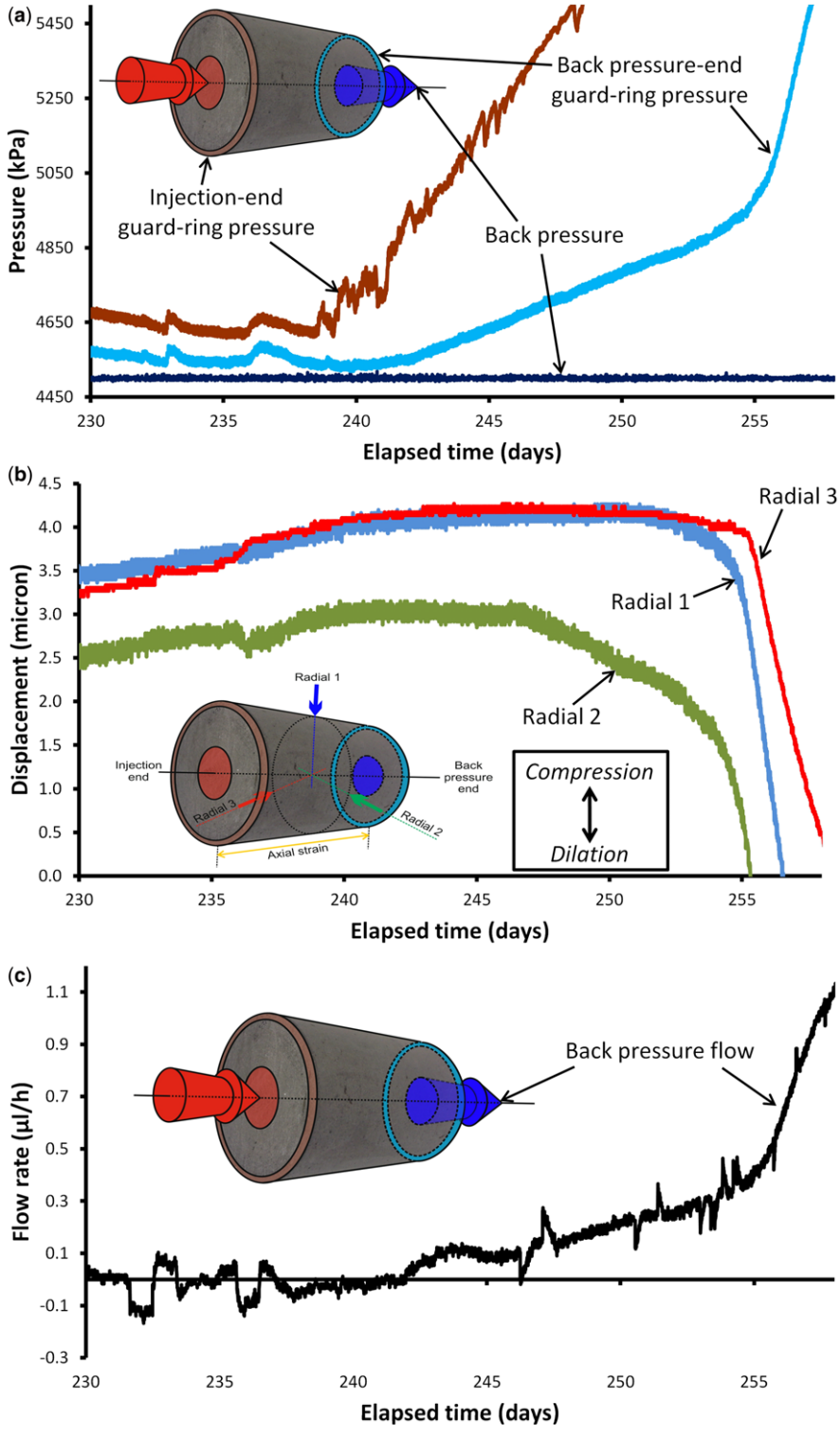

Fig. 5. Detail of data at the onset of gas flow: (**a**) pressure response; (**b**) deformation; (**c**) outflow from the sample.

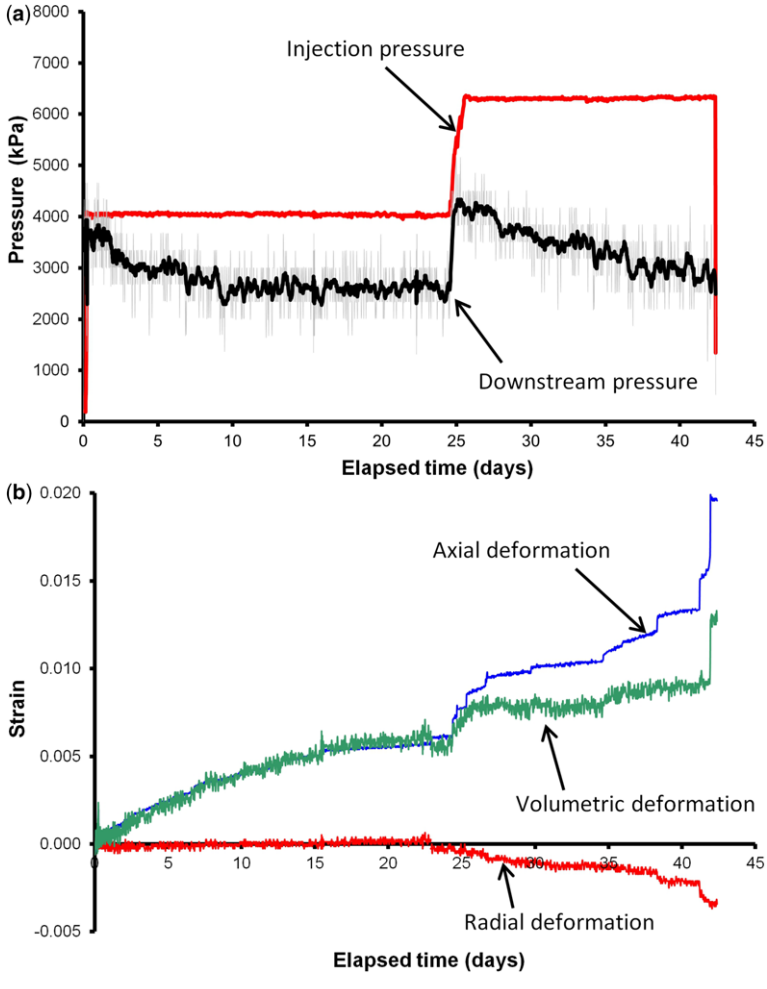

Fig. 6. Experimental results from the LAEGO test: (**a**) gas pressure recorded upstream and downstream of the sample; (**b**) deformation of the sample, clearly showing dilation. Positive strains are extensional/dilational.

acceleration of the axial and lateral strains of the sample until failure.

Discussion

Two independent studies have been conducted specifically to determine the mode of gas propagation in COx. Both studies used a bespoke apparatus designed to measure subtle volumetric strains observed during gas flow experimentation. In the case of BGS, three pressure 'dash-pots' directly measured the radial strain at three points at the midplane of a 56-mm-diameter sample. Axial strain was additionally measured by a digital micrometer. The approach at LAEGO used strain gauges cemented directly to the sample surface, giving axial and lateral strains. In both studies, strains of much less than 1% could be resolved with a high degree of confidence. Both experimental systems were seen to perform effectively and showed marked deformation at the point of gas flow. Both studies clearly show dilational volumetric deformation at the onset of gas flow.

Figure 7 shows the interpretation of the onset of gas migration in COx. A three-stage interpretation has been postulated, which fits all the observations of the BGS and LAEGO, and also previously published results (Horseman *et al.* 1996, 2004; Harrington & Horseman 1999; Angeli *et al.* 2009; Harrington *et al.* 2009, 2012).

Stage 1 (Fig. 7a). The determination of the point of gas entry is a difficult task and one that has eluded many research teams. If gas entry occurs during a

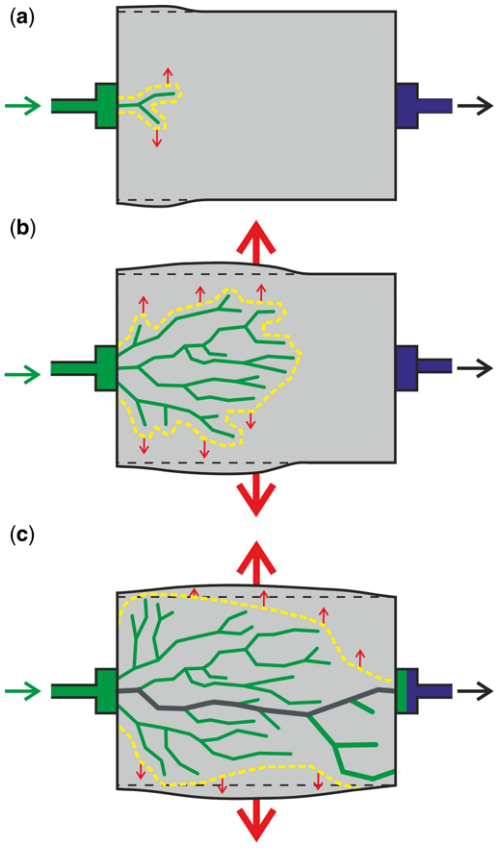

Fig. 7. Interpretation of the onset of gas flow in COx. (**a**) Onset of gas flow when gas started to enter the sample at the injection port. Each gas pathway causes compaction of COx around the pathway, causing bulk sample dilation. (**b**) Dendritic pattern of gas pathways formed, slowly propagating through the sample. Significant dilation was observed at the mid-plane as the pathways propagate past this location. (**c**) Gas migration had reached the backpressure end of the sample as seen in a rise of outflow. As more pathways were opened the sample continued to dilate.

stage of constant injection pressure ramp, it can be inferred by comparing the expected gas pressure from Boyle's Law with the measured pressure. (Boyle's Law states $P_1V_1 = P_2V_2$, where P is pressure and V is volume, so $P_{\text{predicted}} = P_1 \cdot V_1/V$.) At the onset of gas entry, a deviation between the two will occur. However, initial gas entry may only involve small volumes of gas, so the measured pressure may be undiscernibly close to the predicted pressure. If gas entry occurs during a constant pressure stage, the identification of gas flow means that the pressure is greater than the gas entry criteria. Because of the experimental geometry used at the BGS, secondary evidence of gas entry was identified, whereas LAEGO could not identify the pressure at which gas entry occurred.

At about day 220 in the BGS test, gas started to enter the sample when the injection pressure was 10 MPa. Gas migrated as far as the load cell (see Fig. 2b) located on the injection-end platen, where it was identified as an anomalous reading. It is probable that gas migrated along a single bedding layer of the COx as the test sample was oriented parallel to bedding. Gas propagation was along dilatant pathways that exploited the pore network of the material; the pathways can be visualized as 'ruptures' in the pore network. Around each pathway the fabric compressed, which may lead to localized movement of water away from the pathways.

Stage 1a. This stage is derived purely from the geometry of the BGS apparatus. However, it offers insight into gas flow. It is likely that a dendritic pattern of flow pathways was formed, similar in form to that proposed by Hildenbrand *et al.* (2002). At some time, gas migration reached the corner of the sample and interacted with the water-saturated guard rings. As gas entered this sink, water was displaced into the sample until the guard ring was saturated with gas. This resulted in sample swelling and was identified by a slow increase in injection guard-ring pressure. The start of the stage occurred at day 237.32 with a second anomalous reading in the injection-end load cell signifying the movement of gas. Pressure in the guard ring started to increase at day 238.55. A day later, at day 239.8, the first indication of deformation was recorded at the mid-plane array of radial strain measurement devices. This initial strain may have been a consequence of water expulsion from the guard ring and small amounts of sample swelling.

Stage 2 (Fig. 7b). The dendritic network of dilatant pathways propagated further into the sample and reached the mid-plane. In the BGS test this resulted in an acceleration of dilatant deformation around day 255, some 32 days after the first evidence of gas migration. Differences were seen in the timing of the accelerated deformation (see Fig. 5b): radial 2 (day 254), radial 1 (day 254.7), radial 3 (day 255.13), then axial deformation (day 265.03). If all of the observed radial deformation was a result of water being displaced from the guard ring (stage 1b) into the sample, it would be expected that axial deformation would have reacted first. Stage 2 also showed the onset of outflow from the sample, which may have derived from slug flow as gas migrating to the injection-end guard ring resulted in water being expelled into the sample and increased swelling. If all deformation was explained as derived from swelling this would not result in outflow from the sample. Therefore, even though the BGS experimental geometry was likely to result in swelling, the majority of observed

deformation was caused by the dilatant propagation of gas along pathways and cannot be attributed to swelling alone.

Stage 3 (Fig. 7c). Gas had propagated through the sample as far as the backpressure end. The onset of gas reaching the backpressure guard ring (BGS test) at day 273 indicated that gas was now moving throughout the entire length of the sample, although a true steady-state flow had not been achieved, as seen by a mass imbalance between gas entering and exiting the sample. During this stage, the sample continued to slowly dilate, which may indicate that the number of gas pathways was continuing to increase. In the LAEGO test, the increase in upstream gas pressure was immediately followed by an increase in downstream gas pressure, indicating a connection between the ends of the sample. The increase of axial strains seems to show a dilatancy-controlled gas flow, but the low lateral strains suggest that this flow happened in micro-fissures rather than in a major conductive feature. At day 25, with the increase of upstream gas pressure from 4 to 6 MPa, the evolution of downstream gas pressure still suggests a connection between both ends of the sample. At this gas pressure level, the lateral strains began to increase, which suggest, as seen in the BGS test, the initiation in the sample of a major conductive feature (Fig. 7c).

Stage 4. In the LAEGO test, at day 42 the sudden drop in upstream and downstream gas pressures, as well as the sudden increase in axial and lateral strains, seem to show that the major conductive feature resulted in fracturing of the sample, accompanied by gas transport in this tensile fracture (Fig. 1, model iv). The BGS test showed no evidence of gas fracturing. This may indicate that the BGS test was held at a pressure marginally above the gas entry pressure, whereas the second pressure step (6 MPa) in the LAEGO test was greater than the gas entry pressure.

In the BGS test, the acceleration of strain at the mid-plane occurred approximately at day 255, whereas pressure at the backpressure guard ring initiated at day 240.5 (nearly 15 days earlier). This suggests that the backpressure response is a hydromechanical response, whereas the accelerated dilatation is one of gas movement. The pressure increase in the injection pressure guard ring is unstable and this is indicative of gas propagation, whereas the pressure increase at the backpressure guard ring is gradual and suggests that gas had not reached the backpressure end of the sample and is the result of the hydromechanical coupling of the sample. In the LAEGO test, dilatancy-controlled gas flow and gas transport in tensile fractures are barely dissociable, and only the mechanical response of the sample, measured with the strain gauges, allows an understanding of the response of the sample to gas injection. Both research teams have therefore clearly demonstrated that the hydro-mechanical coupling associated with gas movement and the mechanical response of the sample are essential information for fully understanding gas transport mechanisms. The mechanical deformation can be measured either by direct measurement, as in the BGS test using pressure-balanced dash-pots, or by strain gauges directly located on the sample, as in the LAEGO test.

Both experimental studies have shown a strong hydromechanical coupling, which could lead to the question of whether the observed deformation is derived purely as a mechanical response to a change in porewater pressure within the sample. Water is a compressible medium with a bulk modulus of 2.2 GPa. In the BGS test the starting moisture content of the sample was calculated to be 28.7 g (i.e. 28.7 ml), which, given a change in porewater pressure from 4.5 to 10.5 MPa gas pressure (i.e. a change in pore pressure of 6 MPa) would result in 78 μl change in bulk volume of the sample. This is considerably lower than the recorded total sample deformation of 360 μl. In addition, large pressure differentials were seen throughout the test sample, as seen in Figure 4a. Accordingly, the 'bulk sample' does not experience the full 6 MPa change in porewater pressure. A mean pore pressure of 7.9 MPa is observed from the four pressures recorded, giving rise to a change in average pore pressure of 3.4 MPa. This would result in an elastic deformation of 40 μl. Therefore, the full deformation seen by the sample cannot be explained by elastic deformation of the sample water alone. The gas-fracturing of the LAEGO test sample also clearly demonstrates that the strain recorded was not purely derived from elastic deformation of the porewater.

It should be noted that the two independent studies reported here yield significantly different gas entry pressures. The BGS study reports an excess gas entry pressure of 10.5 MPa (backpressure of 4.5 MPa), whereas LAEGO reports 6 MPa (backpressure of *c.* 3 MPa). Similar discrepancies in gas entry pressure for COx have been reported by Davy *et al.* (2012) and have been attributed to micro- or macro-cracking of COx, due to variations in confining pressure, initial sample state or sample preparation method. The sample used by BGS was prepared by machine lathing, whereas the LAEGO sample was prepared by diamond coring. The orientations of the tests samples were also different. For the BGS test the sample was orientated with the long axis parallel to the bedding direction, whereas the LAEGO study was performed perpendicular to bedding. Despite the difference in core orientation, gas injection testing reported by Harrington *et al.* (2012) also gave a high gas entry

pressure similar to that reported here for a sample of COx orientated perpendicular to bedding. Therefore bedding direction does not have a major role in determining gas entry pressures and does not influence the underlying physics governing gas flow.

The current studies have attempted to determine the gas entry pressure, the pressure at which gas can be defined as entering the test sample. The BGS study used a series of pressure ramps and constant pressure stages to observe gas behaviour, whereas the LAEGO study used two constant pressure steps. In the LAEGO test, the two-step approach means that the recorded gas entry and breakthrough pressures are the same. In the BGS test, the gas entry pressure was seen to be 10 MPa, and breakthrough was not seen until a pressure of 10.5 MPa. The gas pressure ramp to increase pressure from 10 to 10.5 MPa was initiated prior to the identification of gas entry and it is uncertain whether gas breakthrough would have occurred at 10 MPa. It can be noted clearly that little difference is observed between gas entry and breakthrough pressures.

Conclusions

Two independent studies have been conducted on COx at the BGS and LAEGO. Both studies were conducted at *in situ* stresses representative of the Bure URL and examined the onset of gas flow through COx. The study conducted at BGS used a bespoke triaxial apparatus specifically designed to be able to resolve very small volumetric (axial and radial) strains potentially associated with the onset of gas flow. The LAEGO study utilized a triaxial setup with axial and radial strains measured by strain gauges glued to the sample. Both studies carefully monitored gas and water flux and pressures throughout long-duration experiments.

A four-stage model has been postulated to explain the experimental results. In stage 1, gas is seen to enter the sample at the gas entry pressure, probably in a dendritic pattern of flow paths. Gas propagation is along dilatant pathways that exploit the pore network of the material, and the pathways can be visualized as 'ruptures' in the pore network. Around each pathway the fabric compresses, which may lead to localized movement of water away from the pathways. In stage 2 the dendritic flow path network has reached the mid-plane of the sample, resulting in an acceleration of radial strain. During this stage, outflow from the sample also develops. In stage 3, gas has reached the back-pressure end of the sample, and free movement of gas occurs from sample end to end. The sample continues to dilate, which may indicate that the number of gas pathways is increasing. Both experimental studies show subtle lateral strain, suggesting that gas flow occurs along micro-fissures rather than in major conductive features (i.e. tensile fractures). Stage 4 represents the gas-fracturing of COx and was only seen in the test conducted by LAEGO. A significant tensile fracture forms, resulting in failure of the sample.

The deformation observed showed considerable hydromechanical coupling. Simple elastic deformation of the porewater could not fully describe the deformation seen by the sample, and the gas-fracturing of the LAEGO experiment clearly demonstrated that gas flow occurred by dilatant pathway formation. The gas entry pressures measured by the two experimental groups provide significantly different gas entry pressures (BGS, 10.5 MPa; LAEGO 6 MPa). This may be explained by differences in sample preparation technique.

Funding for the study was provided by Agence Nationale pour la Gestion des Déchets Radioactifs, Andra (within the auspices of the 'Transfert de Gaz' initiative), the European Atomic Energy Community's Seventh Framework Programme (FP7/2007–2011) under grant agreement no. 230357 (the FORGE project), and the BGS through its well-founded laboratory programme and the Geosphere Containment project (part of the BGS core strategic programme). This paper is published with the permission of the Executive Director, British Geological Survey (NERC).

References

Angeli, M., Soldal, M., Skurtveit, E. & Aker, E. 2009. Experimental percolation of supercritical CO_2 through a caprock. *Energy Procedia*, **1**, 3351–3358.

Askarieh, M. M., Chambers, A. V., Dabniel, F. B. D., Fitzgerald, P. L., Holtom, G. J., Pilkington, N. J. & Rees, J. H. 2000. The chemical and microbial degradation of cellulose in the near field of a repository for radioactive wastes. *Waste Management*, **20**, 93–106.

Autio, J., Gribi, P., Johnson, L. & Marschall, P. 2006. Effect of excavation damage zone on gas migration in a KBS-3H type repository at Olkiluotu. *Physics and Chemistry of the Earth*, **31**, 649–653.

Aziz, K. & Settari, A. 1979. *Petroleum Reservoir Simulation*. Applied Science, London.

Cuss, R. J. & Harrington, J. F. 2010. *Effect of Stress Field and Mechanical Deformation on Permeability and Fracture Self-Sealing: Progress Report on the Stress Path Permeameter Experiment Conducted on Callovo-Oxfordian Claystone*. British Geological Survey Commissioned Report **CR/10/151**.

Cuss, R. J. & Harrington, J. F. 2011. *Update on Dilatancy Associated with Onset of Gas Flow in Callovo-Oxfordian Claystone; Progress Report on Test SPP_COx-2*. British Geological Survey Commissioned Report **CR/11/110**.

Cuss, R. J., Harrington, J. F. & Noy, D. J. 2012. *Final Report of FORGE WP4.1.1: The Stress-path Permeameter Experiment Conducted on Callovo-Oxfordian*

Claystone. British Geological Survey Commissioned Report **CR/12/140**.

DAVY, C. A., M'JAHAD, S., SKOCZYLAS, F., TALANDIER, J. & GHAYAZA, M. 2012. Evidence of discontinuous and continuous gas migration through undisturbed and self-sealed COx claystone. Oral Presentation O/04/2, *Clays in Natural and Engineered Barriers for Radioactive Waste Confinement*, 22–25 October 2012, Montpellier, France.

EKEROTH, E., ROTH, O. & JONSSON, M. 2006. The relative impact of radiolysis products in radiation-induced oxidative dissolution of UO_2. *Journal of Nuclear Materials*, **355**, 38–46.

GALLÉ, C. & TANAI, K. 1998. Evaluation of gas transport properties of backfill materials for waste disposal: H_2 migration experiments in compacted Fo-Ca clay. *Clays and Clay Minerals*, **46**, 498–508.

HARRINGTON, J. F. & HORSEMAN, S. T. 1997. Projects on the effects of gas in underground storage facilities for radioactive waste (Pegasus project): Gas migration in clay. *Proceedings of a Progress Meeting held in Mol, Belgium*, 28–29 May 1997, European Science and Technology Series (1998) EUR 18167 EN, 153–173.

HARRINGTON, J. F. & HORSEMAN, S. T. 1999. Gas transport properties of clays and mudrocks. *In*: APLIN, A. C., FLEET, A. J. & MACQUAKER, J. H. S. (eds) *Muds and Mudstones: Physical and Fluid Flow Properties*. Geological Society, London, Special Publications, **158**, 107–124.

HARRINGTON, J. F., HORSEMAN, S. T. & NOY, D. J. 2003. *Measurements of Water and Gas Flow in Opalinus Clay using a Novel Guard-Ring Methodology*. British Geological Survey Technical Report **CR/03/32**.

HARRINGTON, J. F., NOY, D. J., HORSEMAN, S. T., BIRCHALL, J. D. & CHADWICK, R. A. 2009. Laboratory study of gas and water flow in the Nordland Shale, Sleipner, North Sea. *In*: GROBE, M., PASHIN, J. C. & DODGE, R. L. (eds) *Carbon Dioxide Sequestration in Geological Media—State of the Science*. AAPG, Tulsa, Oklahoma, Studies in Geology, **59**, 521–543.

HARRINGTON, J. F., DE LA VAISSIÈRE, R., NOY, D. J., CUSS, R. J. & TALANDIER, J. 2012. Gas flow in Callovo-Oxfordian Clay (COx): Results from laboratory and field-scale measurements. *Mineralogical Magazine*, **76**, 3303–3318.

HILDENBRAND, A., SCHLÖMER, S. & KROOS, B. M. 2002. Gas breakthrough experiments on fine-grained sedimentary rocks. *Geofluids*, **2**, 3–23.

HORSEMAN, S. T. & HARRINGTON, J. F. 1994. *Migration of Repository Gases in an Overconsolidated Clay*. British Geological Survey Technical Report **WE/94/7**.

HORSEMAN, S. T., HARRINGTON, J. F. & SELLIN, P. 1996. Gas migration in Mx80 buffer bentonite. *In*: *Symposium on the Scientific Basis for Nuclear Waste Management XX (Boston)*. Materials Research Society, **465**, 1003–1010. http://dx.doi.org/10.1557/PROC-465-1003

HORSEMAN, S. T., HARRINGTON, J. F. & SELLIN, P. 1999. Gas migration in clay barriers. *Engineering Geology*, **54**, 139–149.

HORSEMAN, S. T., HARRINGTON, J. F. & SELLIN, P. 2004. Water and gas flow in Mx80 bentonite buffer clay. *In*: *Symposium on the Scientific Basis for Nuclear Waste Management XXVII (Kalmar)*. Materials Research Society, **807**, 715–720. http://dx.doi.org/10.1557/PROC-807-715

KREIS, P. 1991. *Hydrogen Evolution from Corrosion of Iron and Steel in Low/Intermediate Level Waste Repositories*. Nagra Technical Report **NTB 91-21**.

MARSCHALL, P., HORSEMAN, S. & GIMMI, T. 2005. Characterisation of gas transport properties of the Opalinus Clay, a potential host rock formation for radioactive waste disposal. *Oil & Gas Science and Technology – Revue de l'Institute Frances Petrole*, **60**, 121–139.

NERETNIEKS, I. 1984. Impact of alpha-radiolysis on the release of radionuclides from spent fuel in a geologic repository. *Proceedings of the Materials Research Society Symposium*, Boston, MA, 14 November 1983, **26**, 1009–1022. http://dx.doi.org/10.1557/PROC-26-1009

ORTIZ, L., VOLCHARET, G. *ET AL*. 1996. MEGAS Modelling and Experiments on Gas Migration in Repository Host-rocks. Nuclear Science and Technology Series, EUR 16746 EN, Luxembourg, 127–147.

ORTIZ, L., VOLCKAERT, G. & MALLANTS, D. 2002. Gas generation and migration in Boom Clay, a potential host rock formation for nuclear waste storage. *Engineering Geology*, **64**, 287–296.

SMART, N. R., CARLSON, L., HUNTER, F. M. I., KARNLAND, O., PRITCHARD, A. M., RANCE, A. P. & WERME, L. O. 2006. *Interactions Between Iron Corrosion Products and Bentonite*. Serco Assurance Report **SA/EIG/12156/C001**.

WEETJENS, E. & SILLEN, X. 2006. Gas generation and migration in the near field of a supercontainer-based disposal system for vitrified high-level radioactive waste. *In*: *Proceedings of the 11th International High-Level Radioactive Waste Management Conference (IHLRWM)*, Las Vegas, Nevada, 30 April–4 May 2006. American Nuclear Society (ANS), 1–8.

WENK, H.-R., VOLTOLINI, M., MAZUREK, M., VAN LOON, L. R. & VINSOT, A. 2008. *Preferred orientations and anisotropy in shales: Callovo-Oxfordian Shale (France) and Opalinus Clay (Switzerland)*. Clays and Clay Minerals, **56**, 285–306.

WIKRAMARATNA, R. S., GOODFIELD, M., RODWELL, W. R., NASH, P. J. & AGG, P. J. 1993. *A Preliminary Assessment of Gas Migration from the Copper/Steel Canister*. SKB Technical report **TR93-31**.

ZHANG, C.-L., ROTHFUCHS, T., SU, K. & HOTEIT, N. 2007. Experimental study of the thermo-hydro-mechanical behaviour of indurated clays. *Physics and Chemistry of the Earth*, **32**, 957–965.